

Article

Hydrogen's Effect on the Shape Memory Effect of TiNi Alloy Single Crystals

Irina V. Kireeva *, Yuriy I. Chumlyakov, Liya P. Yakovleva and Anna V. Vyrodova

Siberian Physical Technical Institute, National Research Tomsk State University, Lenin Ave. 36, 634050 Tomsk, Russia; chum@phys.tsu.ru (Y.I.C.); liya_petrovna@mail.ru (L.P.Y.); wirodowa@mail.ru (A.V.V.)
* Correspondence: kireeva@spti.tsu.ru; Tel.: +7-960-972-11-75

Abstract: Hydrogen's effect on the shape memory effect (SME) of $[\bar{1}17]$ -oriented $\text{Ti}_{49.7}\text{-Ni}_{50.3}$ (at.%) alloy single crystals, with a B2–B19' martensitic transformation (MT), was studied after being electrolytically hydrogenated at a current density of 1500 A/m² for 3 h at room temperature under isobaric tensile deformation. It was shown that, under the used hydrogenation regime, hydrogen was in a solid solution and lowered the elastic modulus of B19' martensite. The hydrogen in a solid solution increased (i) the yield strength $\sigma_{0.1}$ of the initial B2 phase by 100 MPa at M_d temperature, (ii) the $\sigma_{0.1}$ of the stress-induced B2–B19' MT by 25 MPa at M_s temperature, and (iii) the plasticity of B19' martensite relative to the hydrogen-free crystals. At the same level of external stresses, the SME in the hydrogenated crystals was greater than that in hydrogen-free crystals. At external tensile stresses $\sigma_{\text{ex}} = 200$ MPa, the SME was $4.4 \pm 0.2\%$ in the hydrogenated crystals and $1.8 \pm 0.2\%$ without hydrogen. Hydrogen initiated a two-way SME of $0.5 \pm 0.2\%$ at $\sigma_{\text{ex}} = 0$ MPa, which was absent in the hydrogen-free crystals. The physical reasons leading to an increase in the SME upon hydrogenation are discussed.

Keywords: $[\bar{1}17]$ -oriented Ti-Ni single crystals; shape memory effect; hydrogen; tension



Citation: Kireeva, I.V.; Chumlyakov, Y.I.; Yakovleva, L.P.; Vyrodova, A.V. Hydrogen's Effect on the Shape Memory Effect of TiNi Alloy Single Crystals. *Metals* **2023**, *13*, 1324. <https://doi.org/10.3390/met13071324>

Academic Editor: Ryosuke Kainuma

Received: 8 June 2023
Revised: 4 July 2023
Accepted: 19 July 2023
Published: 24 July 2023



Copyright: © 2023 by the authors. Licensee MDPI, Basel, Switzerland. This article is an open access article distributed under the terms and conditions of the Creative Commons Attribution (CC BY) license (<https://creativecommons.org/licenses/by/4.0/>).

1. Introduction

It is known that alloying with hydrogen atoms leads to a significant change in the properties of metals and alloys, for instance, to a decrease in plasticity at high hydrogen concentrations [1–5], to a decrease or increase in the shear modulus depending on the hydrogenation conditions [1,6], to a change in the strain hardening coefficient, etc. [7–10]. Hydrogen's effect on the deformation becomes especially noticeable when the system approaches the point of concentration or phase transition [1]. In this case, alloys based on titanium nickelide (TiNi) are of particular interest because of their unique shape memory properties [9–20], excellent corrosion resistance [12,18,21], excellent mechanical properties [9,11,12,15], and biocompatibility [1,18,21]. Due to these unique properties, TiNi-based alloys are widely used in medicine as implants and orthodontic wires operating under hydrogen exposure. Since both components (titanium and nickel) of TiNi alloys are hydride-forming metals [1], it is important to know how hydrogenation affects martensitic transformation (MT) temperatures and the mechanical and functional properties of TiNi-based alloys.

By now, hydrogen's effect on MT has been studied mainly on TiNi polycrystals [1,3–8,22–26]. These studies have shown that hydrogen's effect on the mechanical and functional properties is determined by the state of hydrogen in the initial B2 phase (as metal hydrides or atoms in a solid solution), its concentration, and the type of initial phase itself (austenite or martensite) upon hydrogenation. The absorption of hydrogen by the high-temperature B2 phase at 300 K is approximately 2.5 times greater than that by B19' martensite [1]. The main points of the impact of hydrogen on the behavior of TiNi alloys can be summarized as follows. Hydrogen leads to a change in the M_s temperature of the start of the MT (decrease or increase, depending on the conditions of

hydrogenation), to a decrease in the shear modulus of the martensite phase, to an increase in stresses for the onset of stress-induced martensite, and to the formation of oriented martensite. At low concentrations below 400 wppm (wppm represents weight part per million), hydrogen contributes to an increase in the plasticity of the martensite phase and superelasticity. When hydrogen concentrations are greater than 400 wppm, hydrogen reduces plasticity; suppresses shape memory; and in TiNi alloys with a one-stage B2–B19' MT, induces the R phase through stresses [1,3–10,22–26]. Nevertheless, despite numerous experimental data, interest in studying the effect of hydrogen on the functional properties of binary TiNi alloys remains due to their wide use in the dental and medical fields [11,18,21]. In addition, there are no systematic studies in the literature on hydrogen's effect on the shape memory in single crystals of binary TiNi alloys. The advantage of studies using single crystals lies, first of all, in the fact that single crystals make it possible to eliminate the inhomogeneous distribution of hydrogen along grain boundaries and in the grain body and to study in its pure form hydrogen's effect on the shape memory in the crystal body.

The present paper was aimed to study the effect of hydrogen on the shape memory effect (SME) in Ti_{49.7}-Ni_{50.3} alloy crystals with a B2–B19' MT under isobaric tensile deformation in the hydrogen-free state and with hydrogen after hydrogenation at a current density of 1500 A/m² for 3 h at room temperature. The choice of Ti_{49.7}-Ni_{50.3} alloy crystals with a B2–B19' MT was due to the following circumstance. At room temperature, this alloy is in the high-temperature B2 phase [11,12]. This makes it possible to study hydrogen's effect on the properties of the high-temperature B2 phase and the stress-induced B2–B19' MT during the hydrogenation of the high-temperature B2 phase. The choice of the $\bar{1}17$ orientation for studying the SME under isobaric tensile deformation was determined, firstly, by the theoretical value of the lattice deformation $\epsilon_0 = 5.2\%$, which included the deformation of the formation of twinned B19' martensite of $\epsilon_{\text{CVP}} = 2.7\%$ (CVP—correspondence variant pairs) and the deformation through the detwinning of B19' martensite of $\epsilon_{\text{det}} = 2.5\%$ [11,27]. This choice of orientation makes it possible to elucidate hydrogen's effect on detwinning deformation and the magnitude of the SME under isobaric tensile deformation. Secondly, in TiNi alloys, slip deformation in the B2 phase is realized by $\langle 100 \rangle \{110\}$ dislocations [28,29]. The $\bar{1}17$ -oriented crystals have high strength in B2 phase [28–30], and the plastic flow in it during a stress-induced B2–B19' MT is suppressed due to the close to zero Schmid factor $m_{\text{sl}} = 0.13$ for $\langle 100 \rangle \{110\}$ slip systems in this orientation under tension [31]. It was assumed that, under the chosen hydrogenation regime, hydrogen would be in a solid solution and would lead to a change in B2–B19' MT temperatures, an increase in the yield strength of the B2 phase, and an increase in the SME compared to that of the hydrogen-free crystals.

2. Materials and Methods

The Ti_{49.7}-Ni_{50.3} alloy was melted from pure components in an ARC-200 furnace (Arcast Inc., Oxford, MS, USA) with arc remelting in a cold copper crucible. For a uniform distribution of elements over the ingots, the ingots were remelted three times. Single crystals were grown through the Bridgman method in graphite crucibles and helium atmosphere on a Russian-made Redmet installation (Firm "Kristalloomoptika", Tomsk, Russia). The $\bar{1}17$ orientation was determined through the diffractometric method on a DRON-3M X-ray diffractometer (Bourestnik, St.-Petersburg, Russia) with monochromatic Fe K α radiation. Dog-bone-shaped tension samples with a gauge length of 12 mm and a cross section of $2 \times 1.5 \text{ mm}^2$ were cut using wire electrical discharge machining ARTA-5.9 (DELTA-TEST, Fryazino, Moscow region, Russia). The damaged surface layer was removed through chemical etching in $3\text{H}_2\text{O} + 2\text{HNO}_3 + 1\text{HF}$ solution at room temperature. All samples were initially homogenized at 1220 K for 12 h in a quartz tube and a helium atmosphere followed by water quenching. After water quenching, the samples were ground off mechanically, and then they were electrically polished in 490 mL of $\text{CH}_3\text{COOH} + 10 \text{ mL}$ of an HClO_4 electrolyte at 263 K with 20 V applied. The chemical composition of the single crystals after quenching was determined using the X-ray fluorescence method by means of a wavelength dispersive X-ray fluorescence XRF-1800 spectrometer (SHIMADZU,

Kyoto, Japan), giving the atomistic percentages Ti = 49.69% and Ni = 50.31% (at.%). The martensitic transformation (MT) was monitored through differential scanning calorimetry (DSC) (a NETZSCH DSC 404F1 machine with cooling capacity down to ~130 K) (NETZSCH Geratebau GmbH, Selb, Germany) at cooling/heating rates of 10 K/min and on the basis of the temperature dependence of the electrical resistance $\rho(T)$ (a Russian-manufactured installation (Firm “Kristaloptika”, Tomsk, Russia) with a heating/cooling rate of 10 K/min within a temperature range of 77 to 623 K). Starting M_s and finishing M_f temperatures of the forward B2–B19' MT during cooling and starting A_s and finishing A_f temperatures of the reverse B19'–B2 MT during heating were determined through the intersection of tangents on the $\rho(T)$ and DSC curves. The viscoelastic properties of alloy were analyzed using a testing machine for dynamic–mechanical analysis, DMA/SDTA 861e (Mettler Toledo, Columbus, OH, USA), under tension with a maximum strain of 10 μm (working length of 10 mm) at frequencies of 0.1 Hz. Mechanical tests were determined using an Instron 5969 universal testing machine (Instron, Norwood, MA, USA) at a strain rate of $4 \times 10^{-4} \text{ s}^{-1}$. SME under isobaric tensile deformation was studied on home-made dilatometer (Firm “Kristaloptika”, Tomsk, Russia) during cooling and heating in the temperature range of 77 to 400 K at a constant stress in the cycle with a heating/cooling rate of 10 K/min.

The samples were subjected to electrolytic hydrogenation in a thermostated cell in a 0.9% NaCl solution at a current density of 1500 A/m² for 3 h at room temperature. In an aqueous solution, as a result of dissociation, the formation of hydrogen atoms occurred, according to the following reaction:



The hydrogenation time was 3 h at room temperature to obtain the hydrogen concentration necessary to ensure an increase in stresses at the yield point of the B2 phase. The anode was composed of flat-parallel stainless steel plates between which the samples were placed. The samples were the cathode. The hydrogen concentration was measured on a LECO RHEN602 gas analyzer (LECO, St. Joseph, MI, USA). The initial hydrogen content after hydrogenation was 100 ± 20 wppm (~ 100 wppm = 0.01 wt.% ~ 0.5 at.% [7]). After hydrogenation, the samples were placed in a vessel with liquid nitrogen to safekeep hydrogen in them. According to [7,9], under the selected hydrogenation method, hydrogen is in solid solution and does not form hydrides.

The phase composition of the samples after hydrogenation was studied using a JEOL-2010 transmission electron microscope (TEM) (JEOL, Tokyo, Japan) with an accelerating voltage of 200 kV. The thin foils were prepared using double-jet electropolishing (TenuPol-5; “Struers”, Ballerup, Denmark) with an electrolyte containing 20% sulfuric acid in methyl alcohol at room temperature with 12.5 V applied. Thin foils were cut from the samples with hydrogen directly at the edge of the samples containing the hydrogenation product. The samples were thinned from the side of the cut so as to retain the structure after hydrogenation. The fracture surfaces were investigated using a TESCAN VEGA3 scanning electron microscope (SEM) (TESCAN, Brno, Czech).

3. Results and Discussion

3.1. Martensitic Transformation Temperatures before and after Hydrogenation

The B2–B19' MT temperatures of the $[\bar{1}17]$ -oriented Ti_{49.7}Ni_{50.3} (at.%) alloy single crystals in a hydrogen-free state and after hydrogenation are shown in Figure 1. The hydrogen-free Ti_{49.7}Ni_{50.3} single crystals are characterized by a one-stage B2–B19' MT (Figure 1a) [11,12]. The characteristic MT temperatures are shown by arrows. The MT temperatures obtained through three methods show similar values. However, the MT temperatures determined from the DMA curves slightly differ from those obtained from the $\rho(T)$ and DSC curves. This slight difference is due to the different cooling/heating rate during the experiment. Nevertheless, all the used methods show one temperature for

the start of the forward B2–B19' MT upon cooling, $M_s = 285 \pm 5$ K. The experimentally determined M_s temperature of the $\text{Ti}_{49.7}\text{-Ni}_{50.3}$ single crystals is in good agreement with the experimental and theoretical values of the M_s temperature for a nickel concentration of 50.3 at.% in the TiNi alloy for which $M_s = 290$ K [11,12,32,33].

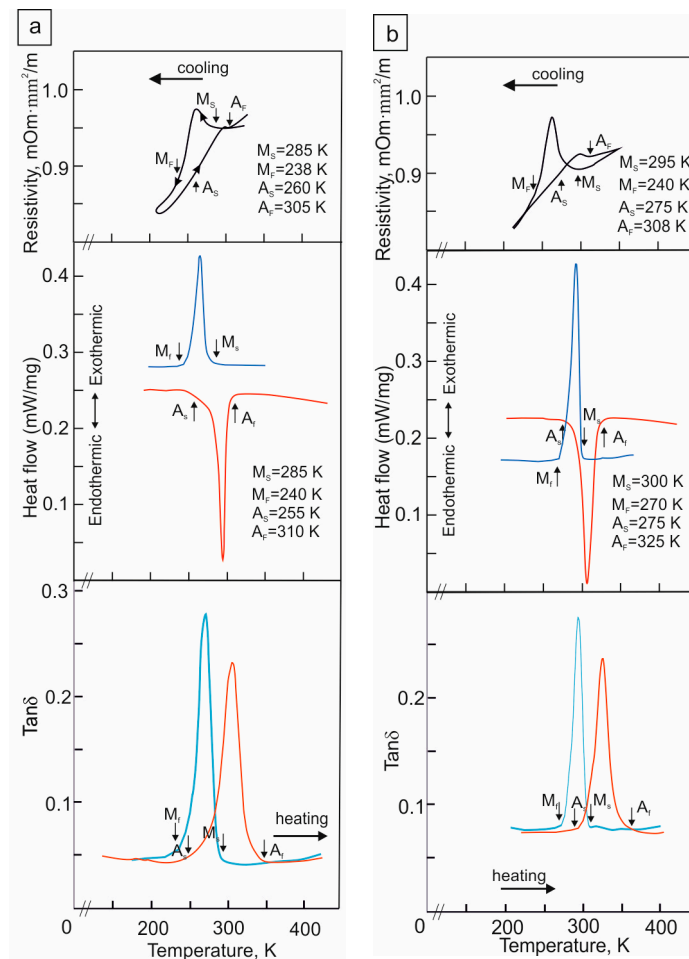


Figure 1. The B2–B19' MT temperatures of the $[\bar{1}17]$ -oriented $\text{Ti}_{49.7}\text{-Ni}_{50.3}$ (at.%) alloy single crystals obtained through three methods: the temperature dependence of the electrical resistance $\rho(T)$, DSC, and DMA curves (a) for hydrogen-free crystals and (b) for hydrogenated crystals; blue line is cooling, red line is heating.

Hydrogenation for 3 h at a current density of 1500 A/m^2 , as shown by the $\rho(T)$, DSC, and DMA curves (Figure 1b), does not change the MT staging relative to the hydrogen-free state but contributes to an increase in the M_s , M_f , A_s and A_f temperatures. This is well demonstrated by the DSC data. It can be seen that the M_s temperature increases by 10 K according to the $\rho(T)$ data and by 15 K according to the DSC curves relative to the hydrogen-free crystals. In contrast to the hydrogen-free crystals, where all three methods give close values for the M_s temperature, after hydrogenation, there is a difference in the M_s determination from the DSC and DMA data relative to the $\rho(T)$ data. The M_s temperature is higher by 5 K according to the DSC data and by 15 K according to the DMA data relative to the $\rho(T)$ data. Such a difference in the determination of the M_s temperature through three methods after hydrogenation is due to different sample sizes as well as the dependence of the mobility and redistribution of hydrogen in the sample volume as a result of different cooling/heating rates during the experiment. After hydrogenation for 3 h at 1500 A/m^2 , the TEM study shows that only reflections of the ordered B2 phase were observed in the microdiffraction patterns. Reflections of the R phase and particles of secondary phases

were not detected (Figure 2). Therefore, it can be assumed that hydrogen is in a solid solution [7,9].



Figure 2. Microdiffraction pattern of the $[\bar{1}17]$ -oriented $\text{Ti}_{49.7}\text{-Ni}_{50.3}$ (at.%) alloy single crystals after hydrogenation, showing only reflexes of the B2 phase. Zone axis $(110)_{\text{B2}}$.

According to the DSC data, where all the MT temperatures are clearly defined, the B2–B19' MT is characterized by overcooling $\Delta M = M_f - M_s$ and overheating $\Delta A = A_s - A_f$, which are, respectively, equal to 45 and 55 K for the hydrogen-free crystals and 30 and 50 K after hydrogenation. A comparison of these values shows that saturation with hydrogen leads to a decrease in the overcooling and overheating. The temperature hysteresis of the hydrogen-free crystals is $\Delta T_h^1 = A_f - M_s = 25$ K and $\Delta T_h^2 = A_s - M_f = 15$ K, and that in the crystals with hydrogen is $\Delta T_h^1 = A_f - M_s = 25$ K and $\Delta T_h^2 = A_s - M_f = 25$ K. It can be seen that, when saturated with hydrogen, ΔT_h^1 and ΔT_h^2 are equal to each other and that the thermal hysteresis is symmetrical in contrast to the hydrogen-free crystals, where $\Delta T_h^1 > \Delta T_h^2$ (Figure 1a). The reverse B19'–B2 MT in the hydrogen-free crystals and those with hydrogen starts at $A_s < M_s$. According to the Tong–Wayman classification, an MT of the second type is observed for which the condition $\Delta G_{dis} < \Delta G_{el}/2$ is satisfied (ΔG_{dis} and ΔG_{el} are dissipated and elastic energy, respectively) [11,12,34,35]. In this case, ΔG_{el} increases with an increase in the transformation strain and, accordingly, the volume fraction of B19' martensite.

Using the thermodynamic description of the MT [35–37] and the experimental values of the MT temperatures determined from the DSC data, it is possible to calculate the values of the stored elastic energy ΔG_{el} for the forward B2–B19' MT and the dissipated energy ΔG_{dis} for the reverse B19'–B2 MT in the $\text{Ti}_{49.7}\text{-Ni}_{50.3}$ crystals without and with hydrogen:

$$|\Delta G_{el}| = T_0 \Delta S_{ch} - (A_s + M_f) \frac{\Delta S_{ch}}{2}; |\Delta G_{dis}| = \frac{\Delta S_{ch}}{2} (A_s - M_f), \quad (2)$$

where $\Delta S_{ch} = 1.953$ J/mol is the entropy change at the B2–B19' MT in the TiNi alloys [11,38]. The estimation of ΔG_{el} and ΔG_{dis} through Relation (2) gives the following values: $\Delta G_{el} = 53.7$ J/mol and $\Delta G_{dis} = 14.6$ J/mol for the hydrogen-free crystals, and $\Delta G_{el} = 48.8$ J/mol and $\Delta G_{dis} = 4.9$ J/mol for the hydrogenated crystals.

It can be seen, firstly, when hydrogenated for 3 h at a current density of 1500 A/m² at room temperature, ΔG_{el} decreases by 4.9 J/mol, and ΔG_{dis} decreases by almost three times relative to the hydrogen-free crystals. This difference in ΔG_{el} and ΔG_{dis} between the hydrogen-free crystals and those with hydrogen can be related to the presence of hydrogen in the solid solution after hydrogenation. Secondly, in the hydrogen-free crystals, $\Delta G_{el}/\Delta G_{dis} = 3.6$, and in the crystals with hydrogen, $\Delta G_{el}/\Delta G_{dis} = 9.9$. This means that hydrogen promotes a reverse B19'–B2 MT and can improve the SME as will be shown below.

3.2. Shape Memory Effect before and after Hydrogenation

The SME during cooling/heating at different levels of external stresses σ_{ex} of the $[\bar{1}17]$ -oriented Ti_{49.7}-Ni_{50.3} alloy single crystals with and without hydrogen is shown in Figure 3. The transformation strain ϵ_{tr} , which is realized in the forward B2–B19' MT under stress during cooling, depending on the level of external tensile stresses σ_{ex} , is shown in Figure 4.

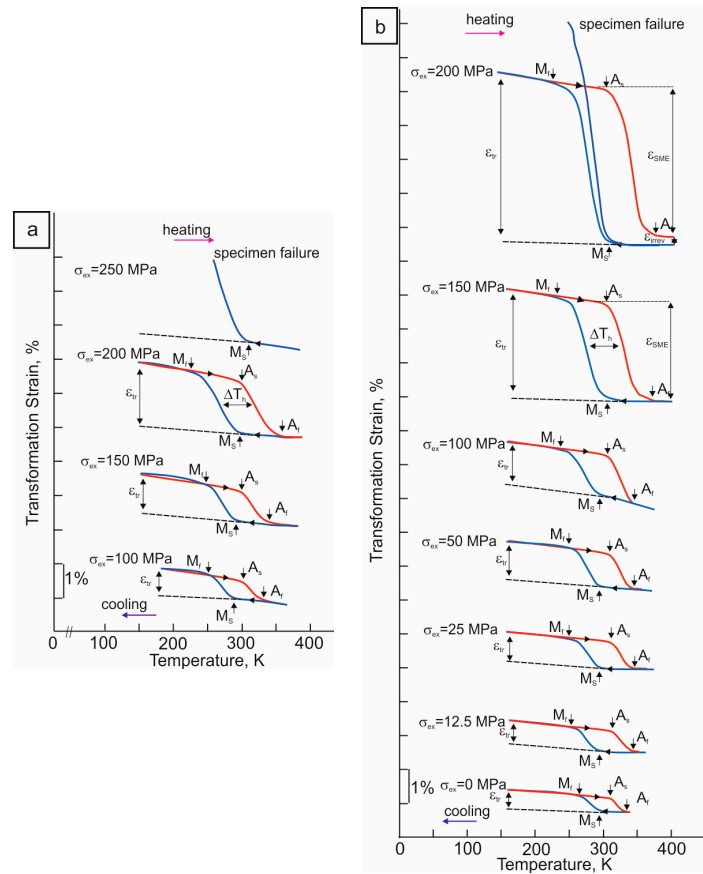


Figure 3. The “transformation strain—temperature” curves under different tensile external stresses of the $[\bar{1}17]$ -oriented Ti_{49.7}-Ni_{50.3} (at.%) alloy single crystals (a) for hydrogen-free crystals and (b) after hydrogenation for 3 h at a current density of 1500 A/m² at room temperature; blue line is cooling, red line is heating.

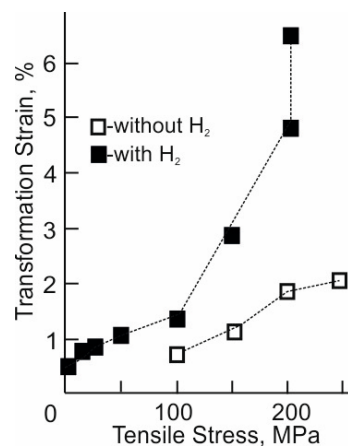


Figure 4. Transformation strain under different tensile external stresses of the $[\bar{1}17]$ -oriented Ti_{49.7}-Ni_{50.3} (at.%) alloy single crystals.

In the hydrogen-free $[\bar{1}17]$ -oriented crystals, the $\varepsilon_{tr}(T)$ curves of the “cooling-heating” cycle under stress have a fully closed form. Hence, the B2–B19' MT, which is realized under stress during cooling, is completely reversible upon heating and exhibits the SME. The first fully closed loop on the $\varepsilon_{tr}(T)$ curve with $\varepsilon_{tr} = 0.7 \pm 0.2\%$ appears at $\sigma_{ex} = 100$ MPa. At $\sigma_{ex} < 100$ MPa, a B2–B19' MT is not determined in the SME experiments under stress. As σ_{ex} increases, ε_{tr} increases, which at $\sigma_{ex} = 200$ MPa reaches $\varepsilon_{tr} = 1.8 \pm 0.2\%$. At $\sigma_{ex} \leq 200$ MPa, an irreversible strain ε_{ir} is not observed on the $\varepsilon_{tr}(T)$ curves. The hydrogen-free $[\bar{1}17]$ -oriented crystals are destroyed at $\sigma_{ex} = 250$ MPa as soon as ε_{tr} under stress during cooling reaches $2.2 \pm 0.2\%$ of strain. It should be noted that this value, $\varepsilon_{tr} = 2.2 \pm 0.2\%$, is less than $\varepsilon_{CVP} = 3.2\%$ for the B2–B19' MT in the crystals of this orientation upon tension [27], and the hydrogen-free $[\bar{1}17]$ -oriented crystals are destroyed before they reach the detwinning deformation ε_{det} of B19' martensite. Therefore, in the hydrogen-free $[\bar{1}17]$ -oriented crystals, the stresses for fracture σ_{fr} are less than the stresses for the detwinning deformation of B19' martensite σ_{det} : $\sigma_{fr} < \sigma_{det}$. Thus, the maximum SME is $\varepsilon_{SME} = 1.8 \pm 0.2\%$, which is less than $\varepsilon_{CVP} = 3.2\%$ for the B2–B19' MT in the crystals of this orientation under tension [27]. It can be seen that, with an increase in σ_{ex} , there is an increase in the M_s temperature under stress and a close to linear increase in $\sigma_{0.1}$ from the temperature, which is characteristic of alloys experiencing a stress-induced MT, which is described by the Clapeyron–Clausius relation [11,12]:

$$\frac{d\sigma_{0.1}}{dT} = -\frac{\Delta S}{\varepsilon_0} - \frac{\Delta H}{\varepsilon_0 T_0}, \quad (3)$$

where ΔS and ΔH are the change in entropy and enthalpy at the B2–B19' MT, T_0 is the phase equilibrium temperature, and ε_0 is the lattice deformation.

In the hydrogenated $[\bar{1}17]$ -oriented crystals, the first fully closed loop on the $\varepsilon_{tr}(T)$ curve with $\varepsilon_{tr} = 0.5 \pm 0.2\%$ appears at $\sigma_{ex} = 0$ MPa (Figure 3b). Upon cooling at $\sigma_{ex} = 0$ MPa, the hydrogenated $[\bar{1}17]$ -oriented crystals begin to spontaneously increase in tensile size. When heated, the sample tensile size is completely restored again. Consequently, the hydrogenated $[\bar{1}17]$ -oriented crystals exhibit a tensile two-way SME [10,11]. The physical reason for the manifestation of a tensile two-way SME in the hydrogenated $[\bar{1}17]$ -oriented crystals can be associated with the appearance of a thin layer of oriented B19' martensite. Oriented B19' martensite arises upon hydrogenation either due to the anisotropic arrangement of hydrogen in the B19' martensite lattice or as a result of the accommodation of the formed B19' martensite in a thin surface layer [5,39,40]. Such an effect was observed even in alloys without the SME up to liquid nitrogen temperature [39]. As σ_{ex} increases, the SME increases. At $\sigma_{ex} = 200$ MPa, the transformation strain under stress reaches the value of $\varepsilon_{tr} = 4.7 \pm 0.2\%$, which is close in magnitude to the theoretical value of the transformation strain of 5.2% for the B2–B19' MT, including ε_{CVP} and ε_{det} , at a given orientation under tension [27]. At $\varepsilon_{tr} = \varepsilon_{CVP} + \varepsilon_{det} = 4.7 \pm 0.2\%$, the irreversible deformation ε_{ir} is 0.3% at $\sigma_{ex} = 200$ MPa. Therefore, the maximum SME is $\varepsilon_{SME} = 4.4 \pm 0.2\%$, which turns out to be $0.8 \pm 0.2\%$ less than the theoretical value $\varepsilon_0 = \varepsilon_{CVP} + \varepsilon_{det} = 5.2\%$ for the B2–B19' MT at the $[\bar{1}17]$ orientation under tension [27]. Upon repeated cooling at $\sigma_{ex} = 200$ MPa, the hydrogenated $[\bar{1}17]$ -oriented crystals reach a strain of $6.5 \pm 0.2\%$ and then are destroyed. In magnitude, this deformation exceeds the theoretical value $\varepsilon_0 = \varepsilon_{CVP} + \varepsilon_{det} = 5.2\%$ for the B2–B19' MT at the $[\bar{1}17]$ orientation under tension [27]. Therefore, hydrogen improves the plasticity of B19' martensite and contributes to ε_{det} . In the hydrogenated $[\bar{1}17]$ -oriented crystals, $\sigma_{fr} > \sigma_{det}$, which is in contrast to the brittle hydrogen-free $[\bar{1}17]$ -oriented crystals for which $\sigma_{fr} < \sigma_{det}$. However, the destruction of the samples at $\varepsilon_{tr} = 6.5 \pm 0.2\%$ does not allow the obtainment of the maximum SME in the hydrogenated $[\bar{1}17]$ -oriented crystals. In the hydrogenated $[\bar{1}17]$ -oriented crystals, the M_s temperature remains unchanged when $\sigma_{ex} = 0$ –100 MPa; additionally, at $\sigma_{ex} > 100$ MPa, it increases under stress, and an almost linear increase in $\sigma_{0.1}$ with temperature is observed, which is described by Relation (3).

A comparison of the ε_{tr} values of the hydrogen-free and hydrogenated $[\bar{1}17]$ -oriented crystals at the same stress level shows that hydrogen leads to an increase in ε_{tr} due to an increase in the plasticity of B19' martensite (Figure 4). Thus, upon hydrogenation, ε_{tr} increases by 2 times at $\sigma_{ex} = 100$ MPa and 2.5–3 times at $\sigma_{ex} = 150$ –200 MPa. An increase in the transformation strain ε_{tr} is due to a decrease in the resistance of the crystal lattice of the alloy to shear deformations because of the “softening” of the shear modulus upon hydrogenation [6,25].

The temperature dependence of the shear modulus $E(T)$ for both the hydrogen-free and hydrogenated $[\bar{1}17]$ -oriented crystals of the $Ti_{49.7}\text{-Ni}_{50.3}$ alloy is shown in Figure 5. It can be seen from Figure 5 that, firstly, in the hydrogenated $[\bar{1}17]$ -oriented crystals, in the test temperature range, the elastic modulus of B19' martensite and the B2 phase is lower than that in the hydrogen-free crystals at the same test temperature. Secondly, with a decrease in the test temperature from 320 to 270 K, the dependence $E(T)$ shows a more pronounced decrease in the elastic modulus in the hydrogenated crystals than in the hydrogen-free crystals. At the M_s temperature, the shear modulus $E(M_s)$ is 24,000 MPa in the hydrogen-free crystals and 20,000 MPa in the hydrogenated crystals. The temperature range in which the “softening” of the modules is observed coincides with the temperature range of the change in internal friction (Figure 5). Consequently, at the moment the M_s temperature is reached during hydrogenation, the crystal lattice of the B2 phase becomes softer than that without hydrogen; it is easily deformed with the formation of a new B19' phase due to the diffusionless process of the displacement of atoms, and the SME improves.

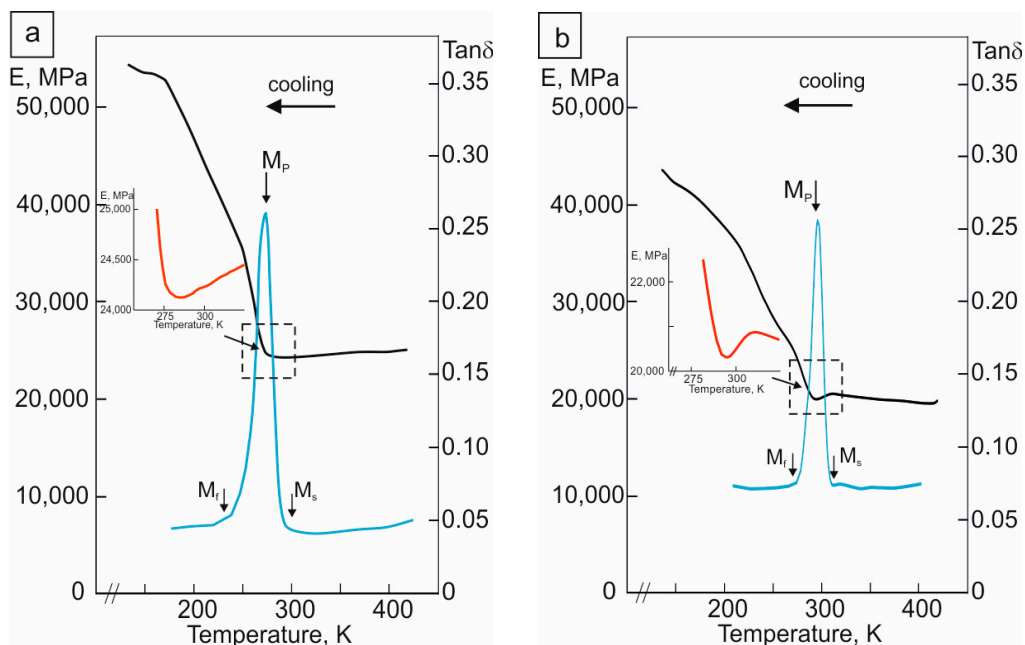


Figure 5. Temperature dependence of elastic modulus $E(T)$ and $\text{Tan}\delta$ of the $[\bar{1}17]$ -oriented $Ti_{49.7}\text{-Ni}_{50.3}$ (at.%) alloy single crystals (a) for hydrogen-free crystals and (b) after hydrogenation for 3 h at a current density of 1500 A/m^2 at room temperature. The selected area of elastic modulus $E(T)$ is shown at a larger scale and is marked in red (inserts of Figures (a,b)); blue color shows the DMA curve ($\text{Tan}\delta$) obtained during cooling.

3.3. Temperature Dependence of Yield Strength before and after Hydrogenation

The temperature dependence of the yield strength $\sigma_{0.1}(T)$ of the $[\bar{1}17]$ -oriented $Ti_{49.7}\text{-Ni}_{50.3}$ alloy single crystals with and without hydrogen within a wide temperature range of 200 to 573 K is shown in Figure 6. Figure 6 additionally displays the value of $\sigma_{0.1}(M_s)$ (filled and unfilled circles) obtained in the SME study under stress (Figure 3). In the temperature range of M_s to 325 K, the $\sigma_{0.1}$ values obtained both in the SME study under

stress and the $\sigma_{0.1}(T)$ dependence are in good agreement with each other. For both the hydrogen-free and hydrogenated crystals, the $\sigma_{0.1}(T)$ dependence exhibits stages, which are usually observed in alloys undergoing a stress-induced MT [11,12]. The minimum stresses on the $\sigma_{0.1}(T)$ dependence are observed at the M_s temperature, which coincides with the M_s value determined from the $\rho(T)$ and DSC curves (Figure 1). The maximum $\sigma_{0.1}$ value corresponds to the M_d temperature at which the stresses for the onset of the stress-induced MT are equal to the stresses for the onset of the plastic flow of the high-temperature B2 phase. The stage at $M_s < T < M_d$ is characterized by an anomalous temperature dependence $\sigma_{0.1}(T)$, which is due to the stress-induced B19'-martensite crystals [11,12]. The $\sigma_{0.1}(T)$ dependence at this stage is described by the Clapeyron–Clausius Relation (3). At $T > M_d$, the $\sigma_{0.1}(T)$ dependence exhibits a stage associated with the plastic deformation of the high-temperature B2 phase.

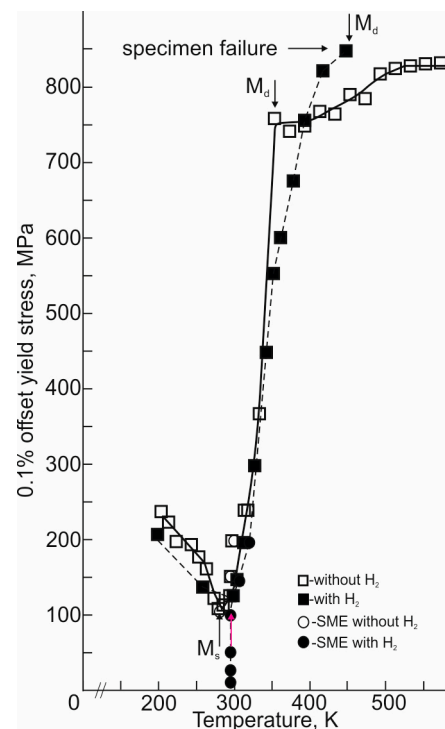


Figure 6. Temperature dependence of 0.1% offset yield stresses of the $[\bar{1}17]$ -oriented $\text{Ti}_{49.7}\text{-Ni}_{50.3}$ (at.%) alloy single crystals under tension. The filled and open circles show the stresses for the onset of stress-induced B2–B19' MT obtained in the SME experiments. The open and filled squares show the 0.1% offset yield stresses obtained in the study of the temperature dependence of $\sigma_{0.1}(T)$ under tension in a wide temperature range.

An analysis of the $\sigma_{0.1}(T)$ dependences shows, firstly, that, upon hydrogenation for 3 h at a current density of 1500 A/m^2 , an increase in the M_s temperature by $12 \pm 2 \text{ K}$ is observed relative to the hydrogen-free crystals. Upon hydrogenation, the increase in the M_s temperature in the study of the $\sigma_{0.1}(T)$ dependence coincides with the increase in the M_s temperature in the study of the $\rho(T)$ and DSC curves (Figure 1). An increase in the M_s temperature upon the hydrogenation of the B2 phase was previously observed in TiNi polycrystals of similar composition under similar hydrogenation conditions [41]. Secondly, in both the hydrogen-free and hydrogenated $[\bar{1}17]$ -oriented crystals, the value $\alpha = d\sigma_{0.1}/dT = 7.5 \text{ MPa/K}$. Therefore, in both cases, the value of $\alpha = d\sigma_{0.1}/dT$ is determined by $\varepsilon_0 = \varepsilon_{\text{CVP}}$, provided that hydrogen under the given hydrogenation conditions has little effect on ΔH and ΔS . Indeed, according to the DSC data, the transformation enthalpy is $15.4 \cdot 10^3 \text{ Jkg}^{-1}$ for the hydrogen-free crystals and $19.85 \cdot 10^3 \text{ Jkg}^{-1}$ for the hydrogenated crystals. If the value of $\alpha = d\sigma_{0.1}/dT$ were determined by $\varepsilon_0 = \varepsilon_{\text{CVP}} + \varepsilon_{\text{det}}$, then in the

hydrogenated $[\bar{1}17]$ -oriented crystals, the $\alpha = d\sigma_{0.1}/dT$ in accordance with Relation (3) would be less since the value of $\alpha = d\sigma_{0.1}/dT$ is proportional to $1/\varepsilon_0$ [11,12]. Thirdly, hydrogenation for 3 h at a current density of 1500 A/m^2 is accompanied by an increase in the M_d temperature and the stresses $\sigma_{0.1}$ for the stress-induced B2–B19' MT at the M_s temperature and the high-temperature B2 phase at $T \geq M_d$. The M_d temperature increases by 100 K, while the $\sigma_{0.1}$ at the M_s and M_d temperatures increases by 25 and 100 MPa, respectively, relative to the hydrogen-free crystals. A similar increase in $\sigma_{0.1}$ at M_s temperature and the B2 phase during electrolytic hydrogenation was previously observed in the $[\bar{1}11]$ -oriented crystals of the $\text{Ti}_{49.3}\text{-Ni}_{50.7}$ alloy when hydrogen was in a solid solution [9].

An important factor indicative of the nature of the distribution of hydrogen in the bulk of the crystals is the fracture surface. The fracture surface of the samples depends on the form in which hydrogen is present in the alloy (as a metal hydride or an atom in a solid solution). If the hydrogen concentration exceeds its solubility limit, then it forms metal hydrides, which are characterized by high brittleness, are preferred sites for the initiation of a brittle crack, and lead to a decrease in plasticity. In the case where the hydrogen concentration does not exceed the solubility limit, hydrogen is in a solid solution, and it leads to deformation localization and increases the plasticity of the alloy [3,5,7,9,24,42]. The fracture surface of the hydrogen-free and hydrogenated $[\bar{1}17]$ -oriented crystals was investigated after the SME experiment at $\sigma_{\text{ex}} = 200\text{--}250 \text{ MPa}$, when the samples were destroyed during the development of a stress-induced MT during cooling (Figure 7).

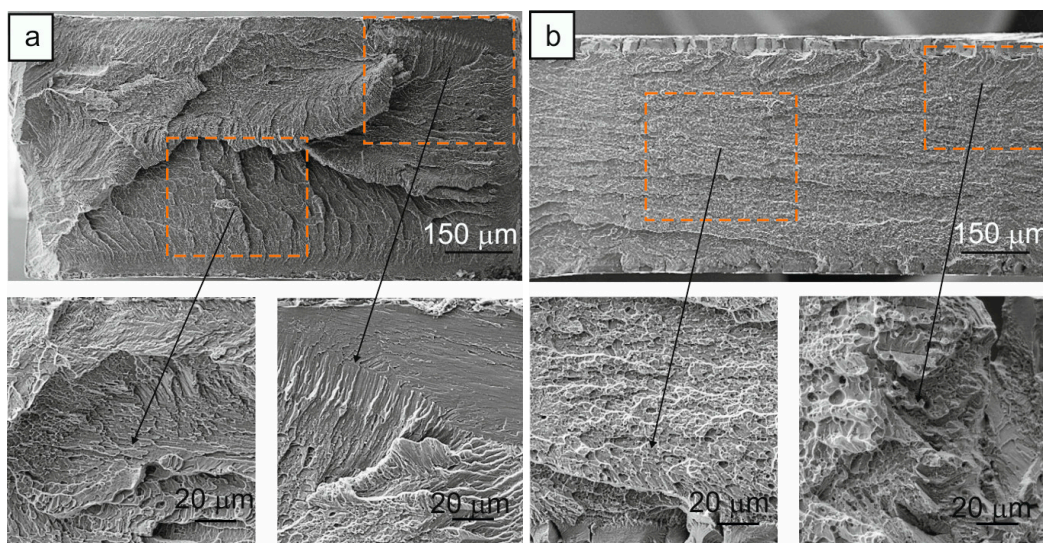


Figure 7. Fracture surface of the $[\bar{1}17]$ -oriented $\text{Ti}_{49.7}\text{-Ni}_{50.3}$ (at.%) alloy single crystals after SME experiment (a) for hydrogen-free crystals at $\sigma_{\text{ex}} = 250 \text{ MPa}$ and (b) after hydrogenation for 3 h at a current density of 1500 A/m^2 at room temperature, $\sigma_{\text{ex}} = 200 \text{ MPa}$. The selected area of fracture surface is shown at a larger scale.

The hydrogen-free crystals exhibit a quasibrittle fracture. On the fracture surface, dimples and cleavage facets are observed, which are characteristic of a quasibrittle fracture (Figure 7a). The hydrogenated crystals are also characterized by a quasibrittle fracture as well as the hydrogen-free crystals. However, the fracture surface of the hydrogenated crystals has a number of differences from the fracture surface of the hydrogen-free crystals: (i) the fracture surface has a localized fracture pattern in one plane with a uniform distribution of small dimples and cleavage facets (Figure 7b); (ii) a brittle layer of $45 \mu\text{m}$ thick is found at the edges of the fracture surface, which is absent in the hydrogen-free crystals. The presence of such a layer indicates an incomplete redistribution of hydrogen in the bulk of the crystals during hydrogenation and its retention on the sample surface. This qualitatively confirms the presence of oriented B19' martensite on the sample surface

after hydrogenation, which initiates a two-way SME during cooling/heating without external stresses and also leads to the fracture process of crystals in the SME experiments at $\sigma_{ex} \geq 200$ MPa. The brittle fracture mechanism characteristic of the presence of hydrides is not observed [24]. Based on the analysis of the fracture surfaces, the increase in $\sigma_{0.1}$ at the M_d temperature, and the literature data [9,24,42], it can be concluded that hydrogen is in the solid solution under the used hydrogenation regime.

Fourthly, in the hydrogenated $[\bar{1}17]$ -oriented crystals of the $Ti_{49.7}-Ni_{50.3}$ alloy, the B2–B19' MT in the SME experiments under stress is determined at low $\sigma_{ex} \leq 100$ MPa, while with respect to the $\sigma_{0.1}(T)$ dependence, $\sigma_{0.1} = 125$ MPa at the M_s temperature (Figures 3 and 7). The TEM study of the hydrogenated $[\bar{1}17]$ -oriented crystals of the $Ti_{49.7}-Ni_{50.3}$ alloy after electrolytic hydrogenation for 3 h at a current density of 1500 A/m² did not reveal either the R phase or particles of secondary phases (Figure 2). Consequently, the development of a B2–B19' MT under $\sigma_{ex} < 100$ MPa in the SME experiments under stress is not associated with the appearance of the R phase. Previously, such a difference between the stresses for the onset of a stress-induced MT under isobaric deformation (SME experiments at different σ_{ex}) and under isothermal deformation (superelasticity experiments and the $\sigma_{0.1}(T)$ dependence) was obtained on single crystals of various orientations of the $(TiZrHf)_{50}Ni_{25}Co_{10}Cu_{15}$ (at.%) high-entropy alloy, [001]-oriented crystals of binary $Ti_{49.4}-Ni_{50.6}$ and $Ti_{49.3}-Ni_{50.7}$ (at.%) alloys, [011]-oriented crystals of the $Ni_{45.3}Ti_{29.7}Hf_{20}Pd_5$ alloy (at.%), and polycrystals of the $Ni_{50.2}Ti_{37.3}Hf_{12.5}$ alloy (at.%) with a thermoelastic B2–B19' MT [43–45]. The physical reason for this difference in stresses was related to the different morphology of martensite: oriented B19' martensite and a mixture of self-accommodated B19' martensite with oriented B19' martensite, respectively, under isothermal and isobaric experiments [43–45]. An analysis of the data presented in [43–45] shows that a different structure at low stresses during isobaric and isothermal deformation is formed in the case where the stresses for the initial B2 phase at the M_d temperature and the stress-induced B2–B19' MT at the M_s temperature have the values, respectively, $\sigma_{0.1}(B2) > 900$ MPa and $\sigma_{0.1}(M_s) > 100$ MPa.

In the hydrogen-free $[\bar{1}17]$ -oriented crystals of the $Ti_{49.7}-Ni_{50.3}$ alloy, $\sigma_{0.1}(B2) = 750$ MPa at the M_d temperature, and $\sigma_{0.1}(M_s) = 100$ MPa is less than in the $(TiZrHf)_{50}Ni_{25}Co_{10}Cu_{15}$, $Ti_{49.4}-Ni_{50.6}$, and $Ni_{45.3}Ti_{29.7}Hf_{20}Pd_5$ alloy single crystals [43–45]. In this case, the minimum stresses for the onset of a stress-induced B2–B19' MT in the SME experiments under stress and $\sigma_{0.1}(M_s)$ on the $\sigma_{0.1}(T)$ dependence turn out to be equal to each other: $\sigma_{ex} = \sigma_{0.1} = 100$ MPa (Figures 3 and 7). Hydrogenation for 3 h at a current density of 1500 A/m² increases the stresses of the B2 phase at the M_d temperature and of the onset of a stress-induced B2–B19' MT at the M_s temperature (Figures 3 and 7). Consequently, hydrogen increases the resistance to the motion of the intervariant and twin boundaries of B19' martensite as compared to those in the hydrogen-free crystals [9]. This, as in the case of the single crystals of the binary $Ti_{49.4}-Ni_{50.6}$ and $Ti_{49.3}-Ni_{50.7}$ alloys and the $(TiZrHf)_{50}Ni_{25}Co_{10}Cu_{15}$ high-entropy alloy [43–45], is the reason that leads to the appearance of a different structure of B19' martensite in the hydrogenated $[\bar{1}17]$ -oriented crystals of the $Ti_{49.7}-Ni_{50.3}$ alloy: mixtures of B19'-martensite (self-accommodated and oriented) under isobaric deformation and oriented B19' martensite under isothermal deformation [43–45].

The elastic energy for the formation of self-accommodated B19' martensite $\Delta G_{el}(SAS)$ is much less than the elastic energy for the formation of oriented B19' martensite $\Delta G_{el}(Or)$ [11,12,36,37,43,46–48]. The stresses for the onset of a stress-induced B2–B19' MT at different contributions of $\Delta G_{el}(SAS)$ and $\Delta G_{el}(Or)$ in the hydrogenated $[\bar{1}17]$ -oriented $Ti_{49.7}-Ni_{50.3}$ crystals, by analogy with [43], can be written in general form according to [11,36,37,46–48]:

$$\sigma_{cr}(T) = \frac{1}{\varepsilon_0(T)} [\Delta G_{ch}(T) + \Delta G_{dis}(T) + \Delta G_{el}(T)]. \quad (4)$$

Here $\Delta G_{ch} = (T - T_0)\Delta S^{A-M}$ is the change in the chemical component of the Gibbs free energy, T_0 is the phase chemical equilibrium temperature, and ΔS^{A-M} is the entropy change at MT. The elastic energy of the B19' martensite structure, consisting of a self-

accommodating structure with a volume fraction f_{SAS} and an oriented structure with a volume fraction f_{or} , of the hydrogenated $[\bar{1}17]$ -oriented $Ti_{49.7}-Ni_{50.3}$ crystals can be written using a mixture rule as follows:

$$\Delta G_{el}^{mix} = f_{SAS}\Delta G_{el}(SAS) + f_{or}\Delta G_{el}(Or) = (1 - f_{or})\Delta G_{el}(SAS) + f_{or}\Delta G_{el}(Or) \quad (5)$$

In the SME experiments σ_{cr} at $\sigma_{ex} < 100$ MPa, it can be determined if, in Relation (4), $\Delta G_{el}(T)$ is replaced by ΔG_{el}^{mix} determined by Relation (5). According to Relations (4) and (5), the $\sigma_{cr}(T)$ increases with increasing σ_{ex} due to an increase in the volume fraction f_{or} of oriented martensite. At $\sigma_{ex} \geq 100$ MPa during the isothermal and isobaric tests, when only oriented B19' martensite is formed, the stressors of $\sigma_{cr}(SME)$ and $\sigma_{0.1}(T)$ at $T \geq M_s$ become equal to each other.

Thus, hydrogenation for 3 h at a current density of 1500 A/m² strengthens the initial B2 phase, increases the stresses for the stress-induced B2–B19' MT at the M_s temperature, increases the plasticity of B19' martensite, and improves the SME.

4. Conclusions

Studies on B2–B19' MTs under stress in $[\bar{1}17]$ -oriented $Ti_{49.7}-Ni_{50.3}$ crystals after electrolytic hydrogenation for 3 h at a current density of 1500 A/m² at room temperature allow us to draw the following conclusions:

1. Hydrogenation for 3 h at a current density of 1500 A/m² at room temperature of the $[\bar{1}17]$ -oriented $Ti_{49.7}-Ni_{50.3}$ crystals does not change the B2–B19' MT type and does not lead to the appearance of the R phase, but it increases the M_s temperature by 10–15 K relative to the hydrogen-free crystals.
2. Hydrogen, when saturated through the electrolytic method at a current density of 1500 A/m² for 3 h at room temperature in the B2 phase, is in a solid solution and leads to a decrease in the elastic modulus $E(T)$ of B19' martensite, an increase in the stress level of the initial B2 phase by 100 MPa at the M_d temperature, and stresses for a stress-induced B2–B19' MT of 25 MPa at the M_s temperature relative to the hydrogen-free crystals.
3. Hydrogen in a solid solution leads to an increase in the SME. At external tensile stresses of 200 MPa, the SME was $1.8 \pm 0.2\%$ in the hydrogen-free crystals and $4.4 \pm 0.2\%$ in the hydrogenated crystals. The physical reason for the increase in the SME is due to an increase in the plasticity of B19' martensite upon hydrogenation. Hydrogen induces a two-way SME of $0.5 \pm 0.2\%$, which is associated with the appearance of oriented B19' martensite in the surface layer after hydrogenation.

Author Contributions: Conceptualization, I.V.K. and Y.I.C.; methodology, I.V.K. and Y.I.C.; validation, I.V.K.; formal analysis, I.V.K. and Y.I.C.; investigation, I.V.K., L.P.Y. and A.V.V.; writing—original draft preparation, I.V.K. and Y.I.C.; writing—review and editing, I.V.K. and Y.I.C.; supervision, Y.I.C.; project administration, I.V.K. All authors have read and agreed to the published version of the manuscript.

Funding: The research was carried out with the support of a grant under the Decree of the Government of the Russian Federation No. 220 of 9 April 2010 (Agreement No. 075-15-2021-612 of 4 June 2021) and by the Tomsk State University Development Program (Priority-2030). Work was conducted with the application of the equipment of the Tomsk Regional Core Shared Research Facilities Center of National Research, Tomsk State University.

Institutional Review Board Statement: Not applicable.

Informed Consent Statement: Not applicable.

Data Availability Statement: Data are available from the corresponding author on reasonable request.

Conflicts of Interest: The authors declare no conflict of interest.

References

1. Spivak, L.V. Synergy effect in the deformation response of thermodynamically open metal-hydrogen systems. *Phys. Usp.* **2008**, *51*, 863–886. [[CrossRef](#)]
2. Robertson, I.M. The effect of hydrogen on dislocation dynamics. *Eng. Fract. Mech.* **1999**, *64*, 649–673. [[CrossRef](#)]
3. Pelton, B.L.; Slater, T.; Pelton, A.R. Effect of hydrogen in TiNi. In Proceedings of the 2nd International Conference on Shape Memory and Superplastic Technologies, SMST-97, Pacific Grove, CA, USA, 2–6 March 1997; pp. 395–400.
4. Yokoyama, K.; Ogawa, T.; Takashima, K.; Asaoka, K.; Sakai, J. Hydrogen embrittlement of Ni-Ti superelastic alloy aged at room temperature after hydrogen charging. *Mater. Sci. Eng. A* **2007**, *466*, 106–113. [[CrossRef](#)]
5. Yokoyama, K.; Kaneko, K.; Ogawa, T.; Moriyama, K.; Asaoka, K.; Sakai, J. Hydrogen embrittlement of work-hardened Ni-Ti alloy in fluoride solutions. *Biomaterials* **2005**, *26*, 101–108. [[CrossRef](#)]
6. Rotini, A.; Biscarini, A.; Campanella, R.; Coluzzi, B.; Mazzolai, G.; Mazzolai, F.M. Martensitic transition in a Ni₄₀Ti₅₀Cu₁₀ alloy containing hydrogen: Calorimetric (DSC) and mechanical spectroscopy experiments. *Scr. Mater.* **2001**, *44*, 719–724. [[CrossRef](#)]
7. Pelton, A.R.; Trepanier, C.; Gong, X.-Y.; Wick, A.; Chen, K.C. Structural and diffusional effects of hydrogen in TiNi. In Proceedings of the ASM Materials & Processes for Medical Devices Conference 2003, Anaheim, CA, USA, 8–10 September 2003; pp. 285–289.
8. Lotkov, A.; Baturin, A.; Grishkov, V.; Rodionov, I.; Kudiyarov, V.; Lider, A. Effect of hydrogen on superelasticity of the titanium nickelide-based alloy. *AIP Conf. Proc.* **2015**, *1683*, 020124. [[CrossRef](#)]
9. Kireeva, I.V.; Chumlyakov, Y.I.; Zakharova, E.G.; Karaman, I. The effect of hydrogen on shape memory effect and superelasticity in single-phase nickel titanium single crystals. *Tech. Phys. Lett.* **2015**, *41*, 284–287. [[CrossRef](#)]
10. Kireeva, I.; Platonova, Y.; Chumlyakov, Y. Effect of hydrogen on the two-way shape memory effect in TiNi single crystals. *Mater. Today Proc.* **2017**, *4*, 4773–4777. [[CrossRef](#)]
11. Otsuka, K.; Wayman, C.M. *Shape Memory Materials*; Cambridge University Press: Cambridge, UK, 1998; p. 284.
12. Otsuka, K.; Ren, X. Physical metallurgy of Ti-Ni-based shape memory alloys. *Prog. Mater. Sci.* **2005**, *50*, 135–678. [[CrossRef](#)]
13. Elahina, M.; Moghaddam, N.S.; Andani, M.T.; Amerinatanzi, A.; Bimber, B.A.; Hamilton, R.F. Fabrication of NiTi through Additive Manufacturing. *Prog. Mater. Sci.* **2016**, *83*, 630–663. [[CrossRef](#)]
14. Moghaddam, N.S.; Saedi, S.; Amerinatanzi, A.; Hinojos, A.; Ramazani, A.; Kundin, J.; Mills, M.J.; Karaca, H.; Elahinia, M. Achieving superelasticity in additively manufactured NiTi in compression without post-process heat treatment. *Sci. Rep.* **2019**, *9*, 41. [[CrossRef](#)]
15. Chumlyakov, Y.I.; Kireeva, I.V.; Saraeva, A.A.; Pobedennaya, Z.V.; Vyrodova, A.V. Effect of the surface oxide layer on shape memory effect and superelasticity of [011]-oriented Ti-50.1Ni single crystals. *Metals* **2022**, *12*, 1932. [[CrossRef](#)]
16. Choi, W.S.; Pang, E.L.; Ko, W.S.; Jun, H.; Bong, H.J.; Kirchlechner, C.; Raabe, D.; Choi, P.P. Orientation-dependent plastic deformation mechanisms and competition with stress-induced phase transformation in microscale NiTi. *Acta Mater.* **2021**, *208*, 116731. [[CrossRef](#)]
17. Sehitoglu, H.; Jun, J.; Zhang, X.; Karaman, I.; Chumlyakov, Y.; Maier, H.J.; Gall, K. Shape memory and pseudoelastic behavior of 51.5% Ni-Ti single crystals in solutionized and overaged state. *Acta Mater.* **2001**, *49*, 3609–3620. [[CrossRef](#)]
18. Ng, C.H.; Chan, C.W.; Man, H.C.; Waugh, D.G.; Lawrence, J. NiTi shape memory alloy with enhanced wear performance by laser selective area nitriding for orthopaedic applications. *Surf. Coat. Technol.* **2017**, *309*, 1015–1022. [[CrossRef](#)]
19. Kireeva, I.V.; Pobedennaya, Z.V.; Chumlyakov, Y.I.; Marchenko, E.S. Effect of stress-induced martensite ageing on the one-way and two-way shape memory effect of [011]-oriented TiNiCu crystals under tension. *Mater. Lett.* **2021**, *305*, 130773. [[CrossRef](#)]
20. Resnina, N.; Belyaev, S.; Liulchak, P.; Karaseva, U.; Bryukhanova, V.; Bikbaev, R.; Palani, I.A.; Prabu, S.S.M.; Manikandam, M.; Jayachandran, S.; et al. Structure, martensitic transformations and mechanical behavior of NiTi shape memory alloy produced by wire arc additive manufacturing. *J. Alloys Comp.* **2021**, *851*, 156851. [[CrossRef](#)]
21. Jani, A.M.; Leary, M. A review of shape memory alloy research application and opportunities. *Mater. Des.* **2014**, *56*, 1078–1113. [[CrossRef](#)]
22. Baturin, A.; Lotkov, A.; Grishkov, V.; Rodionov, I.; Kabdylkanov, Y.; Kudiyarov, V. The effect of hydrogen on martensite transformations and the state of hydrogen atoms in binary TiNi-based alloy with different grain sizes. *Materials* **2019**, *12*, 3956. [[CrossRef](#)]
23. Grishkov, V.; Lotkov, A.; Zhapova, D.; Mironov, Y.; Timkin, V.; Barmina, E.; Kashina, O. Structure and phase state of Ti_{49.4}Ni_{50.6} (at.%) hydrogenated in normal saline. *Materials* **2021**, *14*, 7046. [[CrossRef](#)]
24. He, Y.; Gao, K.W.; Su, Y.J.; Qiao, L.J.; Chu, W.Y. The effect of hydride and martensite on the fracture toughness of TiNi shape memory alloy. *Smart Mater. Struct.* **2004**, *13*, 24–28. [[CrossRef](#)]
25. Skryabina, N.E.; Spivak, L.V.; Fruchart, D. Hydrogen influence on phase transformations in TiNi alloys with shape memory effect. *J. Phys. IV France* **2004**, *115*, 215–221. [[CrossRef](#)]
26. Baturin, A.; Lotkov, A.; Grishkov, V.; Rodionov, I.; Kudiyarov, V. Effect of hydrogen redistribution during aging on structure and phase state of nanocrystalline and coarse-grained TiNi alloys. *J. Alloys Comp.* **2018**, *751*, 359–363. [[CrossRef](#)]
27. Sehitoglu, H.; Hamilton, R.; Canadinc, D.; Zhang, X.Y.; Gall, K.; Karaman, I.; Chumlyakov, Y.; Maier, H.J. Detwinning in NiTi alloy. *Met. Mater. Trans. A* **2003**, *34*, 5–13. [[CrossRef](#)]
28. Chumlyakov, Y.I.; Surikova, N.S.; Korotaev, A. Orientation dependence of strength and plastic properties of titanium nickelide single crystals. *Phys. Met. Metalloved.* **1996**, *82*, 148–158.

29. Kireeva, I.V.; Chumlyakov, Y.I.; Pobedennaya, Z.V.; Saraeva, A.A. Orientation dependence and tension-compression asymmetry of shape memory effect in Ti₅₀Ni₄₀Cu₁₀ single crystals. *Mater. Sci. Eng. A* **2022**, *832*, 142468. [[CrossRef](#)]
30. Chumlyakov, Y.I.; Kireeva, I.V.; Vyrodova, A.V.; Saraeva, A.A.; Pobedennaya, Z.V. Effect of marforming on superelasticity and shape memory effect of [001]-oriented Ni_{50.3}Ti_{49.7} alloy single crystals under compression. *J. Alloys Comp.* **2021**, *896*, 162841. [[CrossRef](#)]
31. Sehitoglu, H.; Karaman, I.; Zhang, X.; Viswanath, A.; Chumlyakov, Y.; Maier, H.J. Strain-temperature behavior of TiNiCu shape memory single crystals. *Acta Mater.* **2001**, *49*, 3621–3634. [[CrossRef](#)]
32. Tang, W.; Sandstron, R. Some aspects on Ti-Ni SMA properties based on calculation of Ti-Ni phase diagram. In Proceedings of the 2nd International Conference on Shape Memory and Superplastic Technologies, SMST-97, Pacific Grove, CA, USA, 2–6 March 1997; pp. 1–6.
33. Tang, W.; Sundman, B.; Sandstron, R.; Qiu, C. New modeling of the B2 phase and its associated martensitic transformation in the Ti-Ni system. *Acta Mater.* **1999**, *47*, 3457–3468. [[CrossRef](#)]
34. Wayman, C.; Tong, H. On the equilibrium temperature in thermoelastic martensitic transformations. *Script. Met.* **1977**, *11*, 3341–3343. [[CrossRef](#)]
35. Tong, H.; Wayman, C.M. Thermodynamics of thermoelastic martensitic transformations. *Acta Met.* **1975**, *23*, 209–215. [[CrossRef](#)]
36. Wollants, P.; Ross, J.R.; Delaey, L. Thermally- and stress-induced thermoelastic transformations in the reference frame of equilibrium thermodynamics. *Prog. Mater. Sci.* **1993**, *199337*, 227–288. [[CrossRef](#)]
37. Palanki, Z.; Daroczi, L.; Beke, D.L. Method for the determination of non-chemical free energy contributions as a function of the transformed alloys. *Mater. Trans.* **2005**, *46*, 978–982. [[CrossRef](#)]
38. Bataillard, L.; Bidaux, J.-E.; Gotthardt, R. Interaction between microstructure and multiple-step transformation in binary NiTi alloys using in-situ transmission electron microscopy observations. *Phil. Mag. A* **1998**, *78*, 327–344. [[CrossRef](#)]
39. Shorshorov, M.H.; Stepanov, I.A.; Flomenblit, Y.M.; Travkin, V.V. Phase and structural transformations caused by hydrogen in alloys based on titanium nickelide. *Phys. Met. Metalloved.* **1985**, *60*, 326–333.
40. Leu, C.-C.; Vokoun, D.; Hu, C.-T. Two-way shape memory effect of TiNi alloys induced by hydrogenation. *Met. Mater. Trans. A* **2002**, *33*, 17–23. [[CrossRef](#)]
41. Stepanov, I.A.; Flomenblit, Y.M.; Zaymovskiy, V.A. Effect of hydrogen on the temperature of thermoelastic martensitic transformation in Titanium Nickel. *Phys. Met. Metalloved.* **1983**, *55*, 612–614.
42. Yokoyama, K.; Ogawa, T.; Asaoka, K.; Sakai, J.; Nagumo, M. Degradation of tensile strength of Ni-Ti superelastic alloy due to hydrogen absorption in methanol solution containing hydrochloric acid. *Mater. Sci. Eng. A* **2003**, *360*, 153–159. [[CrossRef](#)]
43. Chumlyakov, Y.I.; Kireeva, I.V.; Pobedennaya, Z.V.; Yakovleva, L.P.; Vyrodova, A.V.; Kuksgauzen, I.V. Orientation dependence of shape memory effect and superelasticity in (TiZrHf)₅₀Ni₂₅Co₁₀Cu₁₅ high-entropy alloy single crystals. *Shap. Mem. Superelasticity* **2023**, *9*, 300–312. [[CrossRef](#)]
44. Timofeeva, E.E.; Panchenko, E.Y.; Zherdeva, M.V.; Eftifeeva, A.S.; Surikov, N.Y.; Tagiltsev, A.I.; Fatkullin, I.; Tokhmetova, A.; Yanushonite, E.I.; Chumlyakov, Y.I. Shape memory effect in TiNi single crystals with thermal-induced martensite transformation or strain glass transition. *J. Alloys Comp.* **2022**, *922*, 166275. [[CrossRef](#)]
45. Timofeeva, E.E.; Panchenko, E.Y.; Surikov, N.Y.; Tagiltsev, A.I.; Marchenko, E.S.; Chumlyakov, Y.I. On the stress-temperature dependences in TiNi-based shape memory alloys. *J. Alloys Comp.* **2022**, *905*, 164227. [[CrossRef](#)]
46. Tong, H.C.; Wayman, C.M. Characteristic temperatures and other properties of thermoelastic martensites. *Acta Metall.* **1974**, *22*, 887–896. [[CrossRef](#)]
47. Daroczi, L.; Palanki, Z.; Szabo, S.; Beke, D.L. Stress dependence of non-chemical free energy contributions in Cu-Al-Ni shape memory alloy. *Mater. Sci. Eng. A* **2004**, *378*, 274–277. [[CrossRef](#)]
48. Beke, D.L.; Daroczi, L.; Lexcellent, C.; Mertinger, V. Determination of stress dependence of elastic and dissipative energy terms of martensitic phase transformations in a Ni-Ti shape memory alloy. *J. Phys. IV Fr.* **2005**, *115*, 279. [[CrossRef](#)]

Disclaimer/Publisher’s Note: The statements, opinions and data contained in all publications are solely those of the individual author(s) and contributor(s) and not of MDPI and/or the editor(s). MDPI and/or the editor(s) disclaim responsibility for any injury to people or property resulting from any ideas, methods, instructions or products referred to in the content.